Journal of Power Sources 247 (2014) 556–561

Contents lists available at ScienceDirect

Journal of Power Sources

journal homepage: www.elsevier.com/locate/jpowsour

Metal-supported solid oxide fuel cells with impregnated $SrFe_{0.75}Mo_{0.25}O_3$ cathodes

Yucun Zhou*, Xie Meng, Xiaofeng Ye, Junliang Li, Shaorong Wang [1], Zhongliang Zhan [1]

CAS Key Laboratory of Materials for Energy Conversion, Shanghai Institute of Ceramics, Chinese Academy of Sciences (SICCAS), 1295 Ding-xi Road, Shanghai 200050, China

HIGHLIGHTS

- Metal-supported SOFCs were fabricated by tape casting and co-sintering.
- SFMO–YSZ composite cathode was applied by impregnation method.
- Oxygen reduction kinetics of the composite cathode were studied.

ARTICLE INFO

Article history:
Received 11 June 2013
Received in revised form
29 August 2013
Accepted 31 August 2013
Available online 13 September 2013

Keywords:
Metal-supported solid oxide fuel cells
Cathodes
Impregnation
Molybdenum doped strontium ferrite

ABSTRACT

This paper reports on the fabrication in reducing atmospheres of $SrFe_{0.75}Mo_{0.25}O_3$ (SFMO)–8 mol%Y_2O_3-stabilized ZrO_2 (YSZ) composites by impregnating Sr^{2+}-, Fe^{3+}- and $Mo_7O_{24}^{6-}$-containing solutions into the porous YSZ backbones, which would find important applications as cathodes for co-fired metal-supported solid oxide fuel cells. X-ray diffraction examination shows that as-synthesized infiltrates consist of perovskite SFMO oxides and metallic Fe. In situ oxidation during the fuel cell operation eliminates metallic Fe, and SFMO oxides become the predominant component with some minor $SrMoO_4$ impurities. Impedance measurements on symmetric cathode fuel cells show that such impregnated SFMO–YSZ composites exhibit low polarization resistances in air, *e.g.*, 0.06 Ω cm^2 at 800 °C. Metal-supported solid oxide fuel cells, consisting of porous 430L stainless steel substrates, Ni–YSZ active anodes, YSZ electrolytes and impregnated SFMO–YSZ composite cathodes, are fabricated using tape casting, tape lamination, co-sintering and solution impregnation techniques, and show maximum power densities of 438 mW cm^{-2} at 800 °C and 221 mW cm^{-2} at 700 °C.

1. Introduction

Solid oxide fuel cells (SOFCs) electrochemically convert fuels such as hydrogen and methane into electricity in an energetically efficient and environmentally friendly manner. Traditional SOFCs use a thick electrolyte (0.1–1 mm) to support the thin anode and cathode layers. Due to the large ohmic impedance caused by the thick electrolyte, operation temperatures of those electrolyte-supported cells (ESCs) are typically in the range 850–1000 °C. Such high temperatures may bring challenges to the material selection and cell durability. While in the anode-supported cells (ASCs) or cathode-supported cells (CSCs) cases, thick Ni–YSZ anodes or LSM cathodes are used to support the thin electrolytes and the cell working temperature can be reduced to below 800 °C by reducing the ohmic impedance of the electrolyte. However, the mechanical support of both the electrolyte-supported and the electrodes-supported cells is a brittle ceramic or cermet, which is expensive and difficult processed. In contrast, Metal-supported SOFCs (MS-SOFCs) use the electrically conductive and mechanically robust alloys to support the electrochemically active components (including anodes, electrolytes and cathodes) and have shown great promise for reduced materials costs, increased ruggedness and tolerance against rapid thermal cycling [1–12]. Among various alloys, ferritic FeCr stainless steels have been the most widely used as the metallic substrates due to their low costs, compatible thermal expansion coefficients with YSZ electrolytes and adequate resistances against high temperature oxidation [13]. However, interdiffusion of iron, chromium and nickel between ferritic FeCr substrates and nickel-containing anodes has been identified as the main reason for low power densities and rapid

* Corresponding author. Tel.: +86 2169906378; fax: +86 2169906373.
E-mail addresses: zhouyc@student.sic.ac.cn (Y. Zhou), srwang@mail.sic.ac.cn (S. Wang), zzhan@mail.sic.ac.cn (Z. Zhan).
[1] Tel./fax: +86 21 6990 6373.

0378-7753/$ – see front matter
http://dx.doi.org/10.1016/j.jpowsour.2013.08.134

performance degradations of MS-SOFCs, especially when the metallic substrates, Ni-anodes and YSZ electrolytes are co-fired at high temperatures [1]. For example, chromium diffusion depth from CroFer22APU alloys to Ni-anodes could be as large as 60 μm when heat-treated at 1100 °C for 3 h in argon atmosphere [14]. Plasma spray deposition of YSZ electrolytes and electrically conductive diffusion barrier layers such as doped ceria or $La_{0.6}Sr_{0.2}Ca_{0.2}CrO_{3-\delta}$ could improve power densities and durabilities of MS-SOFCs [14,15]. Alternatively, impregnation of nano-scale nickel-containing catalysts into the anode backbone layers could substantially increase their catalytic activities for hydrogen oxidation reactions and thereby allow for reduced-temperature (≈650 °C) operation of MS-SOFCs with reasonably high power densities, which was advantageous in preventing metallic interdiffusion and maintaining good long-term stability [16]. Overall, significant progress has been achieved in the design and fabrication of the anode active layers for MS-SOFCs [1].

For MS-SOFCs with plasma-sprayed electrolytes, the cathode layers are readily deposited using plasma spray and display adequate catalytic activities for oxygen reduction reactions [17–19]. Nevertheless, it becomes much more complicated to select appropriate cathode materials and form highly active cathode layers well bonded to the electrolytes for co-fired MS-SOFCs [1]. The commonly utilized cathode materials such as $La_{1-x}Sr_xMnO_{3-\delta}$ (LSM) and $La_{1-x}Sr_xCo_{1-y}Fe_yO_{3-\delta}$ (LSCF) require sintering in air over the temperature range of 1000–1200 °C, which is not allowed due to excessive oxidation of stainless steel substrates at such high temperatures. On the other hand, decomposition would occur for these cathode materials when sintered in a reducing atmosphere, resulting in unacceptably low performance. In situ sintering during operation has been used to fabricate the cathode layers for co-fired MS-SOFCs, but the resulting cathode polarization resistances are relatively large and may account for half of the total cell resistances. Despite better sinterability at low temperatures of 800 °C, alternative cathode materials such as $Ba_{0.5}Sr_{0.5}Co_{0.8}Fe_{0.2}O_{3-\delta}$ (BSCF) [20] and $SmBa_{0.5}Sr_{0.5}Co_{2.0}O_{5-\delta}$ (SBSCO) [21] have much larger thermal expansion coefficients than the typical electrolyte materials, leading to cracking or delamination of these cathode layers during the thermal cycling. Redox-stable (La, Sr)(Cr, Mn)$O_{3-\delta}$ (LSCM) perovskite oxides were explored as cathodes for MS-SOFCs that could be sintered in nitrogen at 1100 °C, but did not provide sufficient performance at 700–800 °C due to their poor catalytic activity for oxygen reduction reactions [22]. Tucker et al. pioneered impregnation of LSM cathode catalysts into the porous YSZ backbones that was co-sintered with the metallic substrates and the dense YSZ electrolyte layers, obviating the need for high temperature processing, preventing decomposition in non-oxidizing atmospheres and thereby achieving good cathode performance at 650–750 °C [16].

In this work, MS-SOFCs containing porous 430L stainless steel substrates, Ni–YSZ anode active layers, YSZ electrolytes and porous YSZ cathode backbones were fabricated by the tape casting, tape lamination and co-firing techniques. $Sr_2Fe_{1.5}Mo_{0.5}O_{6-\delta}$ (SFMO) was selected as the cathode catalyst due to its good structural stability and important mixed ionic–electronic conducting behavior in both oxidizing and reducing atmospheres [23,24], and was coated onto the internal surfaces of porous YSZ backbones by solution impregnation with subsequent calcinations in reducing atmospheres at 850 °C. The catalytic activities of the resulting SFMO coatings were evaluated after in situ oxidization during the fuel cell operation.

2. Experimental

MS-SOFCs with impregnated SFMO cathodes were fabricated using a two-step procedure. First, metal-supported composite structures, consisting of porous 430L substrates, active Ni–YSZ anodes, dense YSZ electrolytes and porous YSZ backbones, were produced by laminating tape cast green tapes. Powders of 430L stainless steel powders (−400 mesh, Jing-yuan Powder Material Co., Ltd, China) and ammonium oxalate were ball-milled in a weight ratio of 75:25 for 4 h with appropriate amounts of dispersant, binder, plasticizer and solvent. After drying, green 430L-ammonium oxalate sheets of ≈100 μm thick were obtained. Green sheets of YSZ electrolytes, NiO–YSZ anodes and YSZ–ammonium backbones were similarly prepared. Four sheets of 430L-ammonium oxalate, one sheet of NiO–YSZ anodes, one sheet of YSZ and one sheet of YSZ–ammonium backbones were then stacked and uniaxially laminated at 75 °C for 10 min under a pressure of 3000 psi, which were then co-sintered in a reduced atmosphere of 5% H_2/95% N_2 at 1300 °C for 4 h in order to densify YSZ electrolyte layers.

Second, SFMO coatings were deposited into the porous YSZ backbones by impregnating aqueous solutions containing stoichiometric amounts of $Sr(NO_3)_2$, $Fe(NO_3)_3 \cdot 9H_2O$, $(NH_4)_6Mo_7O_{24} \cdot 4H_2O$, where citric acid was also added at a 1:1 M ratio of citric acid to metal ions. After drying, heat treatment was conducted at 850 °C in a reduced atmosphere of 5% H_2–95% N_2 for 2 h to convert these salts into metal oxides without excessive oxidation of 430L substrates. The impregnation/heat treatment cycles were repeated to increase the amounts of impregnated catalysts.

For electrochemical measurements, silver grids were applied onto surfaces of 430L substrates and impregnated SFMO–YSZ cathodes with silver wires attached as the voltage and current leads. Single fuel cells were sealed onto alumina tubes using silver paste (DAD-87, Shanghai Research Institute of Synthetic Resins), and the current–voltage curves were obtained over the temperatures range of 650–800 °C using an IM6 Electrochemical Workstation (ZAHNER, Germany). Ambient air was maintained on the cathodes while 3% H_2O humidified hydrogen was supplied at a flow rate of 100 mL min^{-1} to the anodes. Electrochemical impedance spectras (EIS) were collected at open circuits over the frequency range of 50 mHz–0.2 MHz with a bias voltage of 20 mV. Impedance measurements were also performed in 3% H_2O humidified hydrogen on symmetric anode fuel cells, *i.e.*, 430L|Ni–YSZ anodes|YSZ electrolytes|Ni–YSZ anodes|430L, or in ambient air on symmetric cathode fuel cells, *i.e.*, impregnated SFMO–YSZ|YSZ electrolytes|impregnated SFMO–YSZ. Active area of the single cell, symmetric anode cell and symmetric cathode cell is 0.35, 1.25 and 0.35 cm^2, respectively.

Phase compositions for impregnated SFMO–YSZ composite cathodes, before and after in situ oxidation during the fuel cell operation, were identified at room temperatures using a Rigaku XRD diffractometer with monochromatic CuK_α radiation. The microstructures of fuel cells were examined using scanning electron microscopy (SEM) in Hitachi S-3400N and S-4800-II microscopes. The porosity and pore-size distribution of porous 430L substrates and porous YSZ backbones were measured using mercury intrusion porosimetry carried out with a Micromeritics AutoPore IV 9500 V1.09.

3. Results and discussion

Fig. 1a shows the X-ray diffraction patterns of SFMO–YSZ composites with 40 wt% of SFMO as synthesized in 5% H_2–95% N_2, a relative high loading that would allow for strong X-ray peaks from impregnated catalysts. In addition to the supporting YSZ backbones, diffraction peaks at $2\theta = 32$, 45.86, 56.99 and 66.87 can be ascribed to SFMO perovskite oxides. The diffraction peak at $2\theta = 44.62$ revealed the presence of metallic Fe impurities. Upon in

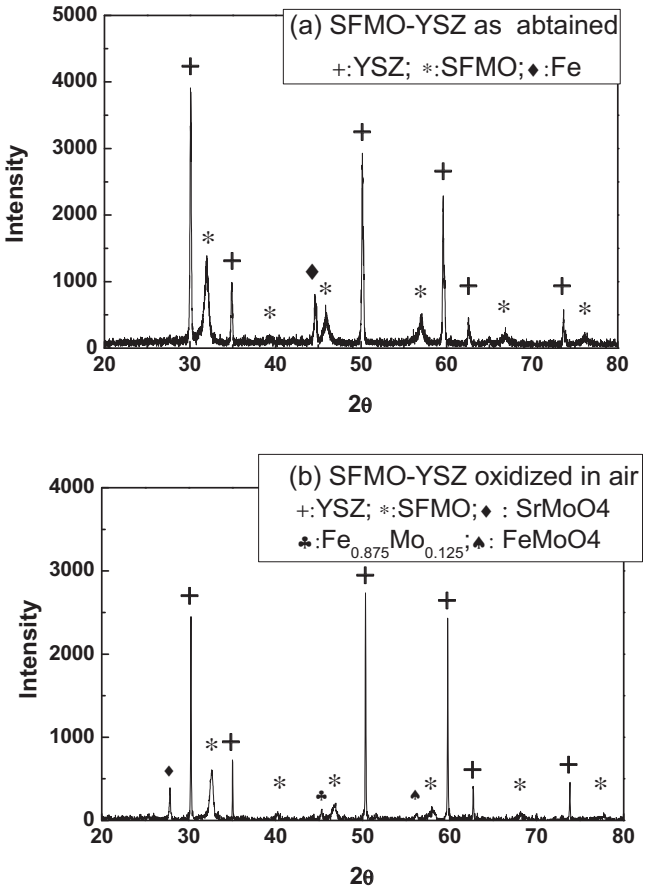

Fig. 1. X-ray diffraction patterns of the SFMO impregnated YSZ cathode: (a) as-synthesized in 5% H_2–95% N_2, and (b) after in situ oxidation in air at 800 °C during the fuel cell operation.

situ oxidation of as-synthesized infiltrates at 800 °C in air during the fuel cell operation, these Fe impurities were completely eliminated whereas SFMO perovskite oxides remained, as shown in Fig. 1b. Furthermore, no diffraction peaks from ferric oxides were observed, indicating that metallic Fe was incorporated into the lattice of SFMO oxides. Nevertheless, another impurity of $SrMoO_4$ appeared as evidenced by a small peak at $2\theta = 27.84$ in Fig. 1b. It is reported that a secondary phase is formed in the mixture of SFMO and YSZ after firing at 1000 °C for 24 h in air [25], however considering the relative lower heat treatment temperature of 850 °C applied in this study, the chemical reaction between YSZ and SFMO may not be the problem. Also, no secondary phase composed of SFMO and YSZ is detected in Fig. 1b.

Fig. 2a shows a representative cross-sectional SEM micrograph of single MS-SOFCs prior to impregnation of SFMO cathode catalysts, consisting of porous 430L substrates, Ni–YSZ active anodes, YSZ electrolytes and porous YSZ backbones. The dense electrolyte was fully dense with a thickness of 16 μm and was well bonded with the adjacent Ni–YSZ active anodes and porous YSZ backbones. The 430L stainless steel substrates were ≈300 μm thick (part of the substrate is not shown in Fig. 2a), providing mechanical strength and collecting the current on the anodes. The average pore size was ≈17 μm and the overall porosity was ≈44%, which allowed for facilitated transport of fuels within the porous alloy substrates. The thicknesses for NiO–YSZ active anodes and porous YSZ backbones were 26 and 60 μm, respectively. A high-magnification SEM micrograph (Fig. 2b) shows that the Ni–YSZ active anodes were much less porous when compared to 430L substrates. Fig. 2a also

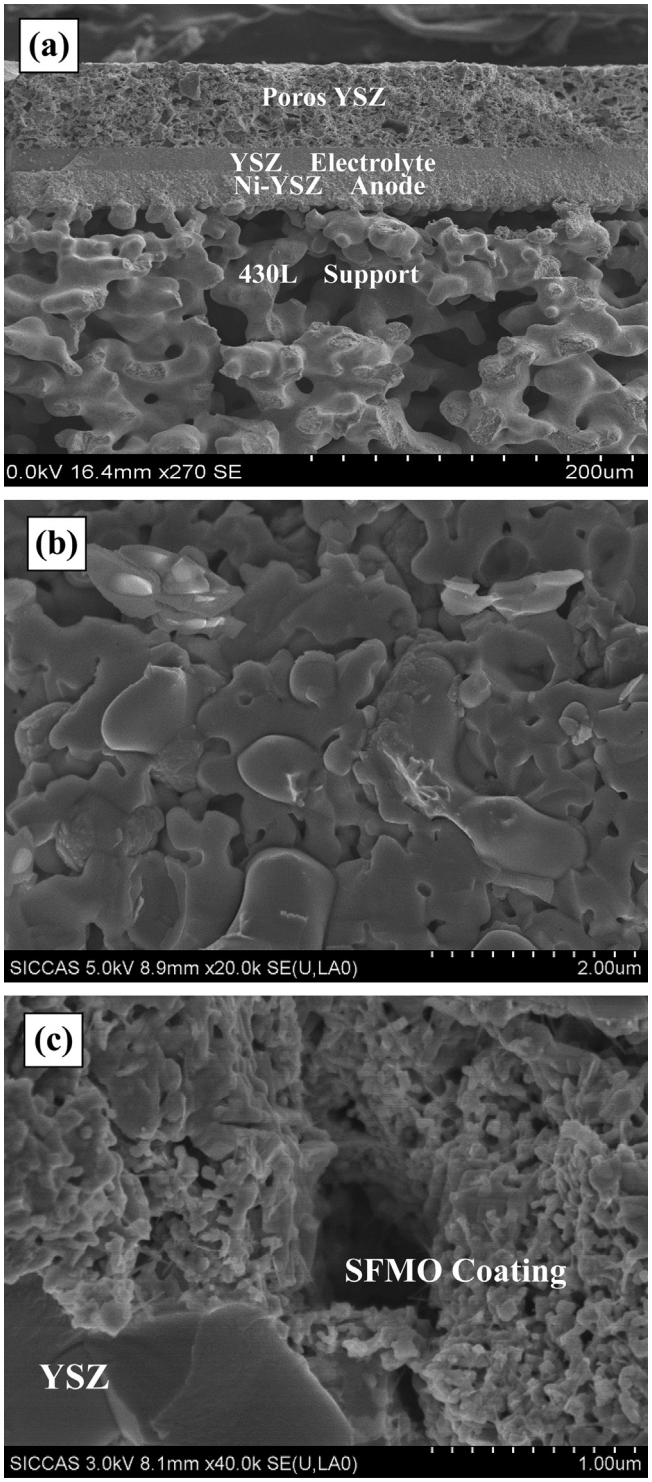

Fig. 2. Cross-sectional scanning electron microscope (SEM) images of the metal-supported SOFCs: (a) The porous 430L support, Ni–YSZ anode, YSZ electrolyte and porous YSZ cathode backbone before impregnation, (b) high-magnification SEM micrograph of Ni–YSZ anode, (c) high-magnification SEM micrograph of SFMO impregnated YSZ cathodes after the fuel cell operation.

shows a homogeneous porous structure for the YSZ backbones with overall porosities of ≈69%. Mercury porosimetry measurements indicated that the porous YSZ backbones exhibited a bi-modal distribution in pore size centered at 1 and 6 μm, respectively. Such porosities and pore structures were advantageous for subsequent impregnation of cathode catalysts. A single impregnation–

calcination cycle yielded an infiltrate loading of ≈5 wt%, and multiple cycles were used to introduce sufficient amounts of infiltrates within the porous YSZ backbones. Fig. 2c shows a high-magnification SEM micrograph of impregnated SFMO–YSZ composite cathodes with 35 wt % of SFMO after fuel cell operation, showing well-interconnected and nanoporous SFMO coatings were deposited onto the internal surfaces of porous YSZ backbones as previously observed for impregnated electrodes [26,27]. The average SFMO particle diameter was ≈60 nm and the mean pore size was ≈40 nm. Such nanoporous SFMO coatings showed great promise as catalytically active cathodes due to their substantially large surface area for oxygen reduction reactions.

Electrochemical characteristics are shown in Fig. 3 for single MS-SOFCs operating on humidified hydrogen fuels and ambient air oxidants at 650–800 °C. Fig. 3a shows typical cell voltages and power densities as a function of current densities. Consistent with gas impermeability of YSZ electrolyte thin films as indicated by the SEM micrograph shown in Fig. 2a, the open circuit voltage (OCV) values were within 50 mV of the thermodynamically expected values and increased from 1.06 V at 800 °C to 1.1 V at 650 °C. The maximum power densities measured were 140, 221, 316 and 438 mW cm^{-2} at 650, 700, 750 and 800 °C, respectively. The current density was 0.56 A cm^{-2} at 0.7 V and 800 °C. In contrast, IMT alloy supported Ni–YSZ anode and YSZ electrolyte fuel cells with diffusion barrier layers and in-situ sintered LSCF cathodes provided higher power density, *i.e.*, 1.064 W cm^{-2} at 0.7 V (820 °C) [12]. Given the high performance of impregnated cathode applied in this study as talked below, such large differences in power densities may be caused by the much thinner YSZ electrolyte (4 μm) and relative porous anode microstructure used in that report.

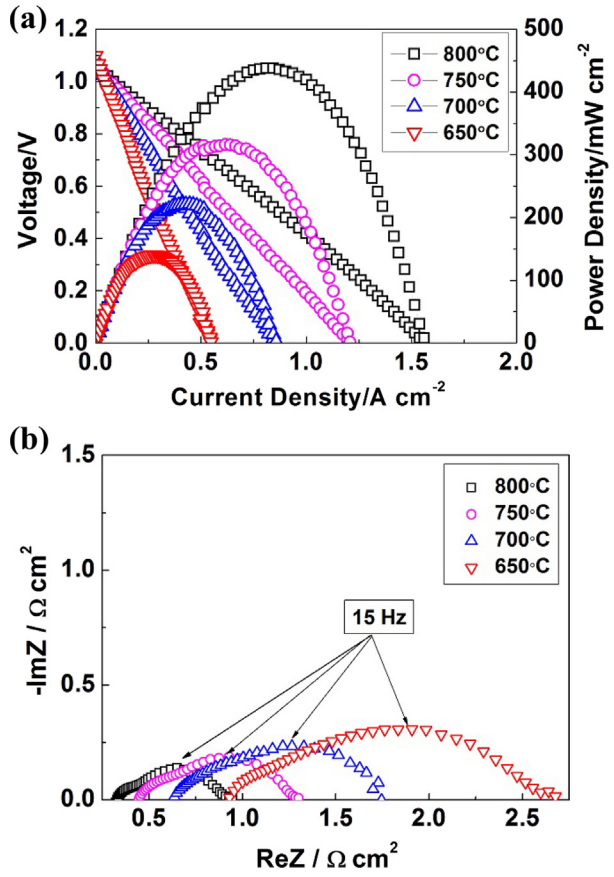

Fig. 3. Electrochemical characteristics of the single fuel cells operating on humidified hydrogen fuels at 100 mL min^{-1} and ambient air oxidants over the temperature range of 650–800 °C: (a) voltage and power density versus current density, and (b) impedance spectras at open circuits.

Fig. 3b shows Nyquist plots of impedance data as obtained at open circuits for the present MS-SOFCs. The ohmic resistance was R_O = 0.33 Ω cm^2 at 800 °C. Based upon the oxide ionic conductivities [28], the area specific resistance for 16 μm-thick YSZ electrolytes can be calculated, *e.g.*, R_{EL} = 0.08 Ω cm^2 at 800 °C. Since the ohmic resistances of the 430L substrates and the active Ni–YSZ anodes were negligibly small, relatively large differences between R_O and R_{EL} might result from the cathode layers, which were not sufficiently conductive due to low conductivities for SFMO oxides [29]. Note that additional contact resistances between different functional layers of single cells might also result in larger than expected ohmic resistances.

Fig. 3b also shows that the combined interfacial polarization resistances ($R_{P,T}$) for single cells, including both the anode and the cathode, were 1.75, 1.08, 0.85 and 0.62 Ω cm^2 at 650, 700, 750 and 800 °C, respectively. These Nyquist plots consisted of small high-frequency arcs and large low-frequency arcs with the respective relaxation frequencies at 1 kHz and 15 Hz. In order to determine the individual contributions of the anode and the cathode to the combined interfacial polarization resistances, symmetric cathode fuel cells in electrolyte-supported configurations, *i.e.*, SFMO–YSZ|YSZ|SFMO–YSZ, and symmetric anode fuel cells in metal-supported configurations, *i.e.*, 430L|Ni–YSZ|YSZ|Ni–YSZ|430L, were constructed with impedance measurements conducted in homogeneous environments over the temperature range of 650–800 °C. Representative Nyquist plots of impedance data at 800 °C are shown in Fig. 4a for symmetric cathode cells in ambient air and in Fig. 4b for symmetric anode cells in 97% H_2–3% H_2O, where the ohmic resistances due to electrolytes and conducting wires were removed while the resistances were divided by 2 to account for contributions of two symmetric electrodes. The cathode polarization resistances were $R_{P,C}$ = 0.06 Ω cm^2 at 800 °C. Despite the presence of minor $SrMoO_4$ impurities as discussed above, the impregnated SFMO–YSZ composites exhibit similar catalytic

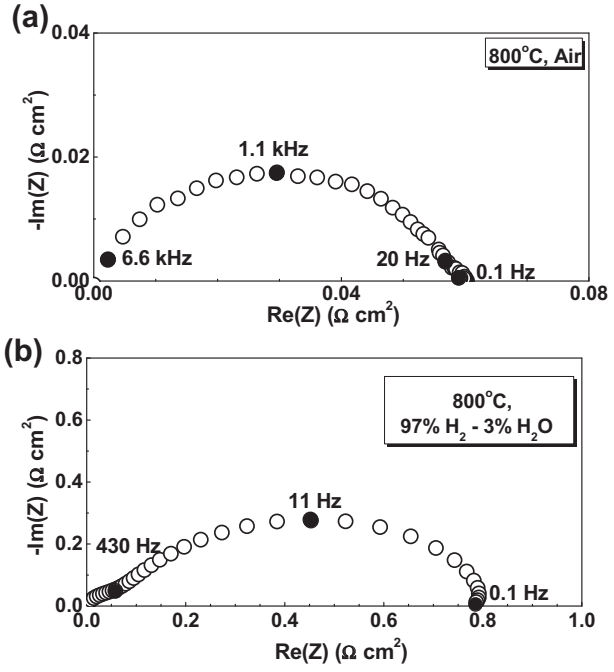

Fig. 4. Nyquist plots of impedance data at 800 °C for (a) symmetric cathode fuel cells in ambient air and (b) symmetric anode fuel cells in humidified hydrogen fuels.

activities for oxygen reduction reactions as alternative impregnated cathodes. For example, the composites of SDC infiltrated SFMO showed $R_{P,C}$ values of 0.11 Ω cm^2 at 750 °C, whereas LSCF and LSF infiltrated YSZ yielded $R_{P,C}$ values of 0.09 and 0.1 Ω cm^2 at 700 °C, respectively [30–32]. Note that the cathode polarization resistances reported here are much lower than for in-situ sintered LSM, LSF, LSCF and SSC cathodes as previously used for metal-supported SOFCs [21]. Irrespective of comparable $R_{P,C}$ values to in-situ sintered SBSC and BSCF oxides [21], the present impregnated SFMO–YSZ composites compare very favorably in terms of adhesions to electrolytes and compatibilities with electrolytes in thermal expansion coefficients.

Fig. 4b shows that the anode polarization resistances were $R_{P,A}$ = 0.79 Ω cm^2 at 800 °C, substantially larger than the value of ≈0.15 Ω cm^2 previously reported at comparable temperatures for Ni–YSZ cermets in anode-supported fuel cells [33]. One possible explanation was metallic interdiffusion between 430L substrates and the Ni–YSZ anode layers during the high temperature co-sintering process that resulted in a dramatical decrease in the anode catalytic activity [13,15]. Additionally, the Nyquist plots for symmetrical anode cells are dominated by the low-frequency arcs centered at ≈11 Hz that have been commonly related to the gas diffusion and adsorption process, indicating that the porosities of the active Ni–YSZ anodes were not sufficiently high and the gas diffusion resistances were relatively large.

The Nyquist plots in Fig. 4a consisted of large high-frequency arcs and small low-frequency arc that are deeply coupled and difficult to deconvolve. In order to gain insights into oxygen reduction kinetics and identify the rate-limiting step, impedance datas were collected for the symmetric cathode fuel cells with 35% of SFMO at 800 °C under varied oxygen partial pressures with the Nyquist plots showed in Fig. 5a. With decreasing oxygen partial pressures, both arcs increased continuously with the low-frequency arc increasingly distinguishable. These impedance data were further fitted with an equivalent circuit, $L(R^H,Q^H)$ (R^L,Q^L), where L was the inductance due to the connecting wires, R^H and R^L were widths of the high- and low-frequency arcs, while Q^H and Q^L were the constant phase elements for the high- and low-frequency arcs, respectively. The resulting R^H and R^L values at varied oxygen partial pressures are summarized in Fig. 5b, showing that R^H increased more pronouncedly than R^L with decreasing oxygen partial pressure. Linear fitting between Log(R_p) and Log(P_{O2}) yielded slopes of 0.37 for R^H and 0.87 for R^L, indicating that the high-frequency arc might be correlated with charge transfer reactions on the SFMO|YSZ interfaces while the low-frequency arc corresponds to oxygen molecule diffusion and adsorption [34]. Given that R^H is more than one order of magnitude larger than R^L for oxygen partial pressures between 0.21 atm and 0.1 atm as shown in Fig. 5b, it can be concluded that oxygen reduction kinetics over impregnated SFMO–YSZ composite cathodes is largely limited by charge transfer reactions on the SFMO|YSZ interfaces.

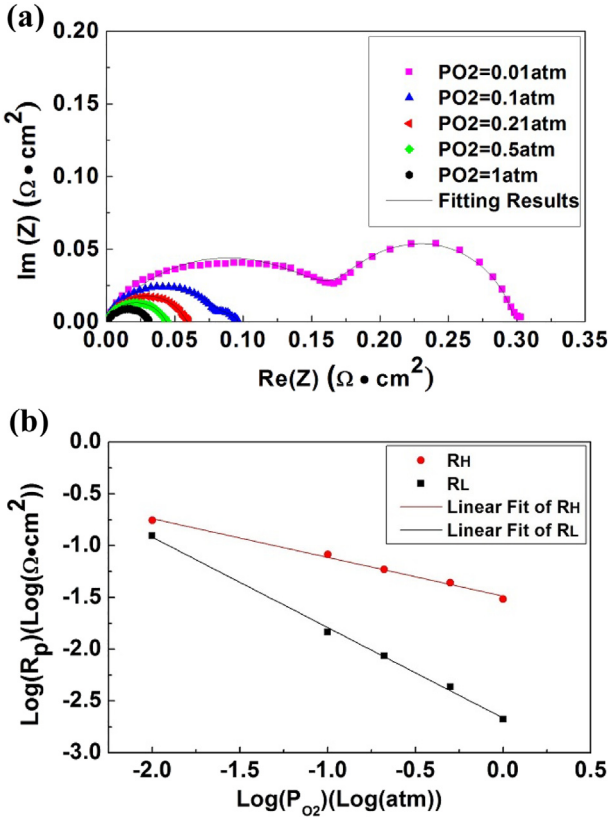

Fig. 5. (a) Nyquist plots of impedance data for symmetric cathode fuel cells with SFMO loadings of 35 wt% measured at 800 °C under different oxygen partial pressures. Included are the fitting results using the equivalent circuit – $L(R^H,Q^H)$ (R^L,Q^L). (b) Dependence of R_H and R_L on oxygen partial pressures at 800 °C.

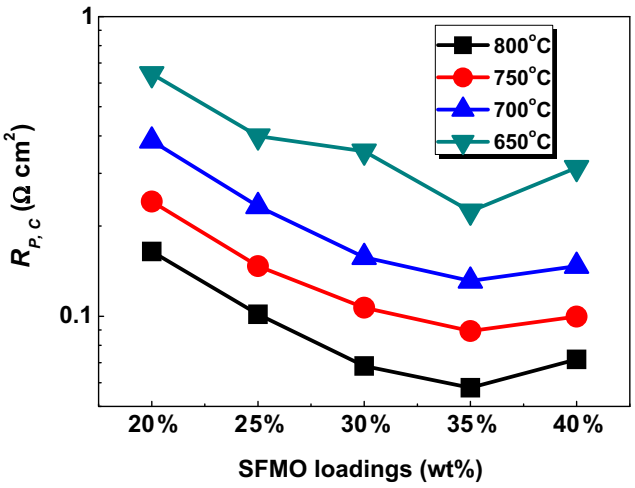

Fig. 6. Effect of SFMO loadings on the polarization resistances of the SFMO impregnated YSZ cathode over the temperature range of 650–800 °C.

Note that tailoring the catalyst loadings is important in reducing the cathode polarization resistance. As shown in Fig. 6, impregnated SFMO–YSZ composites with 35% of SFMO exhibited the lowest polarization resistances at all temperatures between 650 and 800 °C, which is reasonable given that reducing the catalyst loading would result in less surface area available for surface oxygen adsorption and reduced pathways for electron transfer that prevent ionization of adsorbed oxygen atoms [35], whereas increasing the catalyst loading would decrease the overall porosities of the composite cathodes and thereby increase gas diffusion resistances.

4. Conclusions

As an effort to develop high performance cathodes for co-fired metal-supported SOFCs, SFMO–YSZ composites were prepared by impregnating aqueous solutions containing $Sr(NO_3)_2$, $Fe(NO_3)_3$, $(NH_4)_6Mo_7O_{24}$ and citric acid at appropriate ratios into the porous YSZ backbones. Calcinations at 850 °C in reducing atmospheres resulted in predominant formation of perovskite oxides and some Fe minor impurities that were further eliminated via in situ oxidation during the fuel cell operation. Relatively low polarization resistances were achieved in air for the resulting cathodes, *e.g.*, 0.06

and 0.13 Ω cm^2 at 800 and 700 °C, respectively. Analysis of impedance data in varied oxygen partial pressures shows that charge transfer along the SFMO–YSZ interfaces was the rate-limiting step for oxygen reduction reactions on the impregnated SFMO–YSZ cathodes. Metal-supported solid oxide fuel cells, consisting of porous 430L stainless steel substrates, active Ni–YSZ anode layers, YSZ electrolytes and impregnated SFMO–YSZ cathodes, displayed maximum power densities of 438 mW cm^{-2} at 800 °C when operating on hydrogen fuels and air oxidants. Impedance measurements on symmetric anode fuel cells indicate that the fuel cell performance was primarily limited by the large anode polarization resistances due to metallic interdiffusion between the metallic substrates and the Ni-anodes, and possibly low porosities for the active Ni–YSZ anode layers.

Acknowledgment

We gratefully acknowledge the financial support from National Basic Research Program of China (No. 2012CB215401), the National Natural Science Foundation of China (No. 51172266, 51072219), Chinese Government High Tech Developing Project (2011AA050702), Science and Technology Commission of Shanghai Municipality (No. 09DZ1206600, 11PJ1410300), Science and Technology Commission of Zhejiang Province under contract No. 2011C16037, and the 100 Talents Program of Chinese Academy of Sciences.

References

[1] M.C. Tucker, J. Power Sources 195 (2010) 4570–4582.
[2] A. Ansar, P. Szabo, J. Arnold, Z. Ilhan, D. Soysal, R. Costa, A. Zagst, M. Gindrat, T. Franco, in: S.C. Singhal, K. Eguchi (Eds.), Solid Oxide Fuel Cells, vol. 12, 2011, pp. 147–155.
[3] M. Ruettinger, R. Muecke, T. Franco, O. Buechler, N.H. Menzler, A. Venskutonis, in: S.C. Singhal, K. Eguchi (Eds.), Solid Oxide Fuel Cells, vol. 12, 2011, pp. 259–268.
[4] P. Blennow, J. Hjelm, T. Klemenso, S. Ramousse, A. Kromp, A. Leonide, A. Weber, J. Power Sources 196 (2011) 7117–7125.
[5] R. Leah, A. Bone, A. Selcuk, D. Corcoran, M. Lankin, Z. Dehaney-Steven, M. Selby, P. Whalen, in: S.C. Singhal, K. Eguchi (Eds.), Solid Oxide Fuel Cells, vol. 12, 2011, pp. 351–367.
[6] M.C. Tucker, G.Y. Lau, C.P. Jacobson, L.C. DeJonghe, S.J. Visco, J. Power Sources 175 (2008) 447–451.
[7] L.M. Rodriguez-Martinez, M. Rivas, L. Otaegi, N. Gomez, M.A. Alvarez, E. Sarasketa-Zabala, J. Manzanedo, N. Burgos, F. Castro, A. Laresgoiti, I. Villarreal, in: S.C. Singhal, K. Eguchi (Eds.), Solid Oxide Fuel Cells, vol 12, 2011, pp. 445–450.
[8] R. Hui, J.O. Berghaus, C. Deces-Petit, W. Qu, S. Yick, J.-G. Legoux, C. Moreau, J. Power Sources 191 (2009) 371–376.
[9] Y.-M. Kim, P. Kim-Lohsoontorn, S.-W. Baek, J. Bae, Int. J. Hydrogen Energy 36 (2011) 3138–3146.
[10] Y.-W. Ju, H. Eto, T. Inagaki, S. Ida, T. Ishihara, J. Power Sources 195 (2010) 6294–6300.
[11] C.-S. Hwang, C.-H. Tsai, J.-F. Yu, C.-L. Chang, J.-M. Lin, Y.-H. Shiu, S.-W. Cheng, J. Power Sources 196 (2011) 1932–1939.
[12] T. Franco, M. Haydn, R. Muecke, A. Weber, M. Ruettinger, O. Buechler, S. Uhlenbruck, N.H. Menzler, A. Venskutonis, L.S. Sigl, in: S.C. Singhal, K. Eguchi (Eds.), Solid Oxide Fuel Cells, vol. 12, 2011, pp. 343–349.
[13] I. Villarreal, C. Jacobson, A. Leming, Y. Matus, S. Visco, L. De Jonghe, Electrochem. Solid-State Lett. 6 (2003) A178–A179.
[14] M. Brandner, M. Bram, J. Froitzheim, H.P. Buchkremer, D. Stover, Solid State Ionics 179 (2008) 1501–1504.
[15] T. Franco, K. Schibinger, Z. Ilhan, G. Schiller, A. Venskutonis, ECS Trans. 7 (2007) 771–780.
[16] M.C. Tucker, G.Y. Lau, C.P. Jacobson, L.C. DeJonghe, S.J. Visco, J. Power Sources 171 (2007) 477–482.
[17] G. Schiller, R.H. Henne, M. Lang, R. Ruckdäschel, S. Schaper, Fuel Cells Bull. 3 (2000) 7–12.
[18] D. Soysal, A. Ansar, Z. Ilhan, R. Costa, in: S.C. Singhal, K. Eguchi (Eds.), Solid Oxide Fuel Cells, vol. 12, 2011, pp. 2233–2241.
[19] D. Waldbillig, O. Kesler, J. Power Sources 191 (2009) 320–329.
[20] Y.-M. Kim, J. Bae, ASME Conf. Proc. 2009 (2009) 847–849.
[21] S.-W. Baek, J. Jeong, Y.-M. Kim, J.H. Kim, S. Shin, J. Bae, Solid State Ionics 192 (2011) 387–393.
[22] S.-W. Baek, J. Jeong, S. Lee, J. Bae, ECS Trans. 25 (2009) 2909–2914.
[23] A.B. Munoz-Garcia, M. Pavone, E.A. Carter, Chem. Mater. 23 (2011) 4525–4536.
[24] A.B. Munoz-Garcia, D.E. Bugaris, M. Pavone, J.P. Hodges, A. Huq, F. Chen, H.-C. zur Loye, E.A. Carter, J. Am. Chem. Soc. 134 (2012) 6826–6833.
[25] Q.A. Liu, X.H. Dong, G.L. Xiao, F. Zhao, F.L. Chen, Adv. Mater. 22 (2010) 5478–5482.
[26] Z.L. Zhan, D. Han, T.Z. Wu, X.F. Ye, S.R. Wang, T.L. Wen, S. Cho, S.A. Barnett, RSC Adv. 2 (2012) 4075–4078.
[27] D. Han, X.J. Liu, F.R. Zeng, J.Q. Qian, T.Z. Wu, Z.L. Zhan, Sci. Rep. UK 2 (2012).
[28] J.W. Fergus, J. Power Sources 162 (2006) 30–40.
[29] G.L. Xiao, Q. Liu, S.W. Wang, V.G. Komvokis, M.D. Amiridis, A. Heyden, S.G. Ma, F.L. Chen, J. Power Sources 202 (2012) 63–69.
[30] L. Zhang, Y. Liu, Y. Zhang, G. Xiao, F. Chen, C. Xia, Electrochem. Commun. 13 (2011) 711–713.
[31] J. Chen, F.L. Liang, L.N. Liu, S.P. Jiang, B. Chi, J. Pu, J. Li, J. Power Sources 183 (2008) 586–589.
[32] Y.Y. Huang, J.M. Vohs, R.J. Gorte, J. Electrochem. Soc. 151 (2004) A646–A651.
[33] J.R. Wilson, W. Kobsiriphat, R. Mendoza, H.Y. Chen, J.M. Hiller, D.J. Miller, K. Thornton, P.W. Voorhees, S.B. Adler, S.A. Barnett, Nat. Mater. 5 (2006) 541–544.
[34] G. Xiao, Q. Liu, F. Zhao, L. Zhang, C. Xia, F. Chen, J. Electrochem. Soc. 158 (2011) B455–B460.
[35] J.M. Vohs, R.J. Gorte, Adv. Mater. 21 (2009) 943–956.